Electrochimica Acta 464 (2023) 142936

Contents lists available at ScienceDirect

Electrochimica Acta

journal homepage: www.journals.elsevier.com/electrochimica-acta

β-cyclodextrin based platform for bimodal detection of o-toluidine and cholesterol: Electrochemical and fluorescence sensing

Wafa Aidli [a,b,*], Valentina Pifferi [a], Abdelmoneim Mars [b], Daniele Marinotto [c], Mariangela Longhi [a], Amedea Manfredi [a], Ahmed Hichem Hamzaoui [b], Luigi Falciola [a,**]

[a] Dipartimento di Chimica, Università degli Studi di Milano, via Golgi 19, 20133 Milano, Italy
[b] Valorization Laboratory of Useful Materials (LVMU), National Center of Material Science Research (CNRSM), Techno-park Borj Cedria, 8027 Solima, Tunisia
[c] Institute of Chemical Sciences and Technologies "Giulio Natta" (SCITEC) of CNR, via Golgi 19, 20133 Milano, Italy

ARTICLE INFO

Keywords:
Benzoquinone
Cyclodextrins
Cholesterol
Dual-mode sensing
Graphene
Host-guest inclusion
o-toluidine
Graphene quantum dots

ABSTRACT

A novel dual-mode sensor based on the in-situ coupling of electrochemical (EC) and fluorescence (FL) assay for o-toluidine and cholesterol detection is reported. The detection platform was constructed by assembling nitrogen doped graphene quantum dots (N-GQDs), benzoquinone (BQ) and β-cyclodextrin (β-CD). Once the analyte is captured by β-CD, a concentration-depended variation of the electrochemical and fluorescence signals occurs. Based on this meticulous design, low electrochemical ($LOD_{o\text{-Toluidine}} = (5.53 \pm 0.16)$ μM; $LOD_{cholesterol} = (2.10 \pm 0.042)$ μM) and fluorescence ($LOD_{o\text{-Toluidine}} = (5.06 \pm 0.15)$ μM; $LOD_{cholesterol} = (2.95 \pm 0.23)$ μM) detection limits were achieved. In addition, the platform showed good selectivity in the presence of various interfering agents as well as long storage stability. Finally, the proposed method was applied to detect cholesterol in processed cow milk as a real sample, with apparent recoveries between 93.18% and 102,91%.

1. Introduction

Over the past two decades, there has been a growing demand for rapid, highly sensitive, and selective analytical tools to address new challenges in environmental monitoring [1,2], food safety [3], and public health [4]. In response to this demand, researchers have focused on the development of analytical and sensing techniques, especially chemical sensors, which have attracted much attention not only because of their low cost and ease of use, but for the great improvements they have achieved in terms of sensitivity and selectivity [5].

As chemical sensors, we have witnessed the evolution of various transduction modes mainly electroanalytical techniques, including electrochemical (EC), electrochemiluminescent (ECL), and photoelectrochemical (PEC) methods in parallel with optical sensors essentially fluorescence (FL), colorimetric (CL), surface-enhanced Raman scattering (SERS), surface plasmon resonance (SPR) and chemiluminescence strategy.

Although each method has its own advantages, its application is still not problem-free. Since most analytical sensors rely on a single signal to quantify analytes, they are susceptible to interference and matrix effects in real samples, resulting in low accuracy in their practical application [6]. To overcome these concerns, the ratiometric approach with multiple signal responses has proven to be an appealing and promising solution for more precise analytical tools.

Ratiometric sensors employ two independent signals, and their ratio is used as the final readout. The ratiometric strategy originated with fluorescence and chemiluminescence sensors where multiple fluorescent probes are used on the same system and their signals are integrated as a final readout [7]. In the last years, the concept has been introduced also to electrochemical applications [8]. Sensors with inner reference electroactive probes were developed. In this kind of sensors, the presence of multiple readout signals provides an intrinsic built-in correction factor to eliminate the contribution from non-specific interferences [9].

From the same perspective, numerous researchers got inspired to create bimodal sensors. With advances in modern material science, researchers have taken advantage of the different properties of nanomaterials to develop sensors that combine different transduction modes for instance electrochemistry–colorimetry [10], electrochemistry–electrochemiluminescence [11,12], electrochemistry–photoelectrochemistry [13–15], fluorescence and electrochemistry [16–18], and fluorescence–colorimetry

* Corresponding author at: Dipartimento di Chimica, Università degli Studi di Milano, via Golgi 19, 20133 Milano, Italy.
** Corresponding author.
E-mail addresses: wafa.aidli@unimi.it (W. Aidli), luigi.falciola@unimi.it (L. Falciola).

https://doi.org/10.1016/j.electacta.2023.142936
Received 20 February 2023; Received in revised form 12 July 2023; Accepted 22 July 2023
Available online 26 July 2023

[19]. By utilizing two or more sensing modes, bimodal sensors provide cross-validation of the detected analyte. The ability to verify the presence and concentration of a target analyte through different sensing modes significantly enhances reliability in the obtained measurements [20].

This new class of sensors is still in its early stages of development, thus novel approaches for extending dual-signal readout sensing applications are greatly appreciated.

In this regard, we attempt to design a new dual-mode sensor that combines electrochemistry and fluorescence transduction modes by means of an assembly of nitrogen doped graphene quantum dots (N-GQDs), benzoquinone (BQ) and β-cyclodextrins (β-CD).

N-GQDs were chosen as fluorescent probe. Among different fluorescent nanomaterials, N-GQDs were distinguished not only by their pronounced optical and electrical properties [21], but also by their mild preparation conditions [22], high photostability, excellent biocompatibility, good water-solubility, and low toxicity [23]. These unique physicochemical properties make them potential candidates for optical/electrochemical applications.

On the other hand, benzoquinone was adopted as an electrochemical probe.

Due to their low redox potential, chemical stability, and reversibility toward electron transfer in aqueous buffers, the two-electron and two-proton *p*-hydroquinone/*p*-benzoquinone (H_2Q/BQ) has been well studied as organic electrochemically active label [24]. The stable electrochemical activity of BQ was exploited for their application as redox probe in sensors, biosensors [25] and redox flow batteries [26].

Finally, to guarantee the selectivity of the sensor, β-cyclodextrins (β-CDs) were employed as recognition units. With their truncated cone-shaped and hydrophobic central cavity, β-CDs can form noncovalent inclusion complexes by interacting selectively with various molecules. Thus, β-CDs were widely used in sensors design [27].

As illustrated in Scheme 1, BQ is expected to produce a redox electrochemical signal (EC), while the N-GQDs will generate a fluorescence signal (FL) under excitation. In the proposed sensing platform, host gest inclusion complex is expected to vary the EC-FL signals proportionally to the concentration of the target molecules. By combining electrochemical and fluorescence sensing techniques, the platform will allow a mutual verification of the presence and concentration of o-toluidine and cholesterol. This mutual verification reduces the likelihood of false positives or false negatives, ensuring accurate and reliable detection results.

Taking o-Toluidine and cholesterol as electroactive and electroinactive model targets, a dual-mode sensor with an EC-FL response is established. The choice of the above-mentioned target molecules is based on their relevance and high affinity toward β-cyclodextrin. Hypercholesterolemia, or excessive levels of cholesterol in the blood, increases the risk of cardiovascular disease, which is a leading cause of death worldwide [28]. Food accounts for around 25% of the cholesterol in our blood [29]. As a preventive precaution, dietary cholesterol intake tracking is crucial. Thus, food cholesterol determination is essential. o-Toluidine, on the other hand, is classified as an emerging pollutant that poses serious threats to public health and the environment [30,31] . Human exposure to o-Toluidine is caused by dyes and pigments manufacturing, rubber production, as well as tobacco smoking which consider the primary source to o-Toluidine in humans [32]. The International Agency for Research on Cancer (IARC) recently has classified o-Toluidine as a potential human carcinogen producing urinary bladder cancers, raising the urgency of its monitoring [33].

2. Experimental part

2.1. N-doped graphene quantum dots synthesis

Nitrogen doped graphene quantum dots were prepared according to the literature [23,34]. Briefly, 1 g of citric acid and 0.25 g Tris-HTMA were heated in a 5 mL beaker at 160 °C. The molten substance color changed from colorless to pale yellow, and then to orange after 15 min heating, indicating the formation of N-GQDs. After that, 0.5 M of NaOH solution was dropped in the obtained orange liquid under vigorous stirring condition to reach pH 7.

2.2. Step by step sensor design

The designed sensor was fabricated in a stepwise process as shown in Scheme 2. More experimental details are included in the Supporting Materials.

First, fluorine tin oxide (FTO) electrodes (20 mm × 25 mm × 1.1 mm) were cleaned ultrasonically with ethanol and water for 2 times in sequence. Then, the cleaned and dried FTO electrodes were sonically treated in a 10% NaOH solution for 10 min to obtain hydroxylated active FTO surface.

For the silanization of the electrode, chemical vapor deposition procedure was adopted [35]. The activated FTO glasses were placed in glass container together with a Teflon cup containing 200 µl 3-Aminopropyl)triethoxysilane (APTES). The container was then placed in an oven at 100 °C for 1 h. The FTO/APTES electrodes were then rinsed with ethanol (3 times) to remove non-bonded silane molecules from the glass surface and dried at 105 °C for 30 min. Meanwhile, N-GQDs suspension

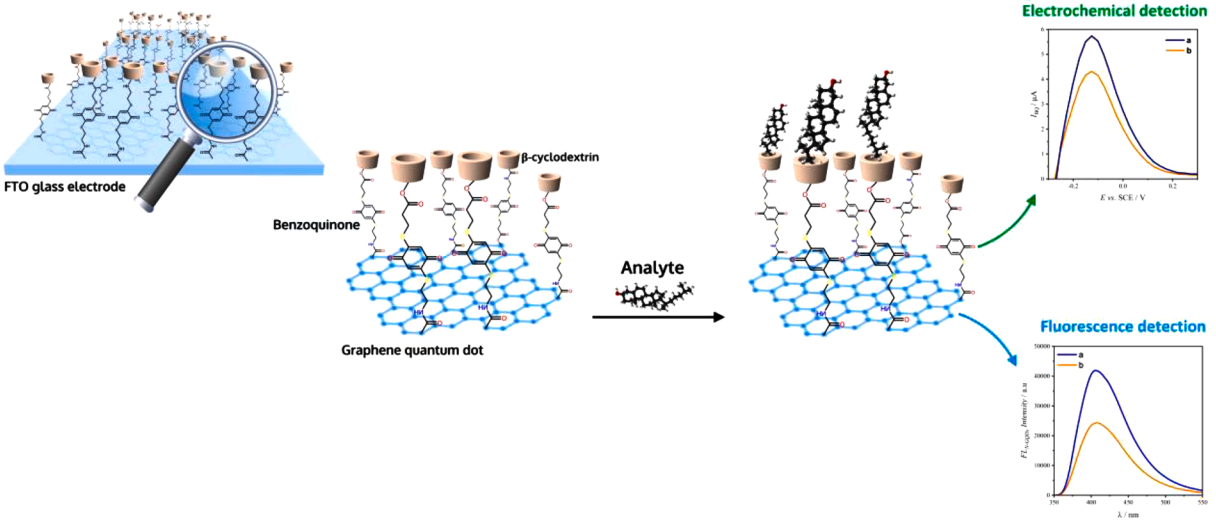

Scheme 1. Working principle of the bimodal sensor by the coupling of EC and FL assays.

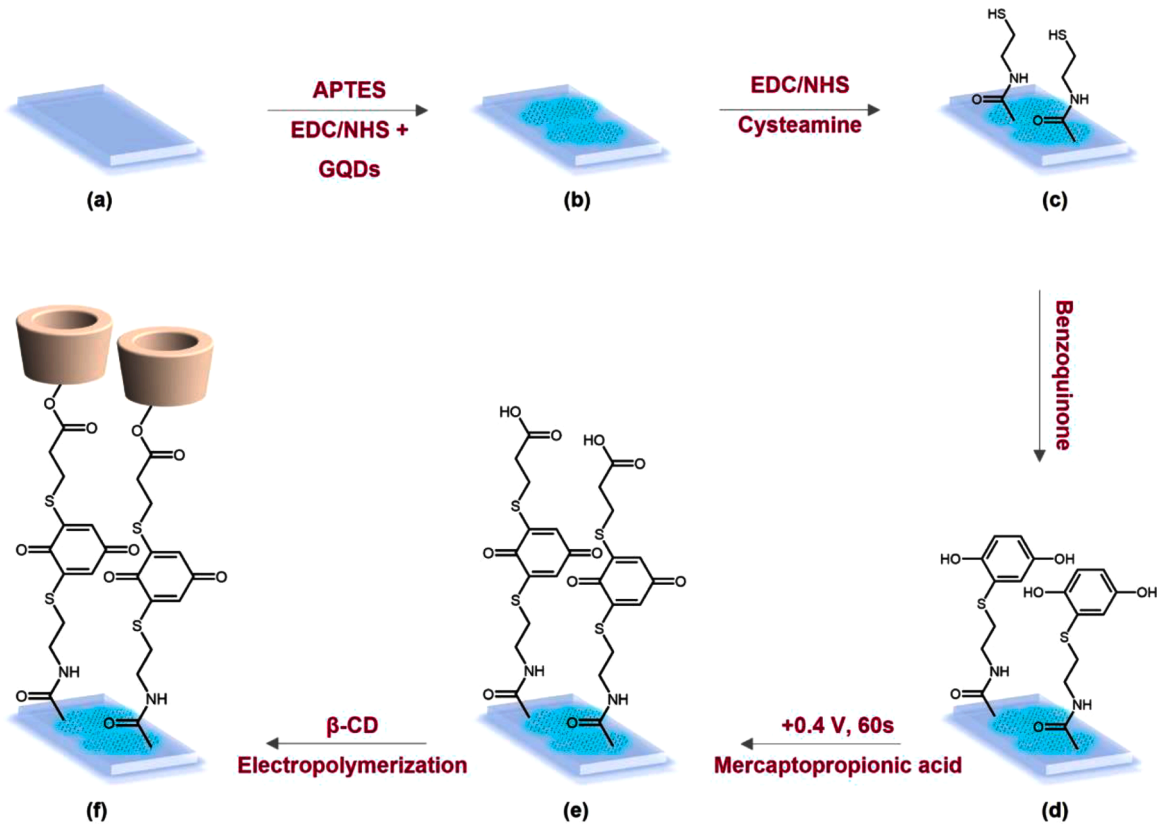

Scheme 2. Schematic illustration of the construction of the dual-mode sensing platform: (a) bare FTO electrode (b) N-GQDs/APTE/FTO, (c) Cys/N-GQDs/APTE/FTO, (d) BQ/Cys/ N-GQDs/APTE/FTO, (e) COOH/ BQ/Cys/ N-GQDs/APTE/FTO, (f) β-CD/ COOH/ BQ/Cys/ N-GQDs/ APTE/FTO.

was activated by adding 1-ethyl-3-(3-dimethylaminopropyl)-carbodiimide (EDC, 10 mM) and n-hydroxysuccinimide (NHS, 20 mM) in dark for 30 min. Following, ITO/APTES electrodes were immersed in the N-GQDs solution for 4 h to obtain N-GQDs coated FTO electrode.

Benzoquinone anchoring was achieved by Michael addition. First, N-GQDs/APTES/FTO electrode was incubated in a 5 mM cysteamine aqueous solution for 2 h to create a thiol-terminated monolayer. Next the electrode was washed and incubated in a 5 mM benzoquinone aqueous solution for 1 h [33].

For β-cyclodextrins grafting, 3-mercaptopropanoic acid was used as a linker between benzoquinone and cyclodextrins. First, it was found that an electrooxidation process were necessary to restore the oxidative structure of benzoquinone [34,35]. For that, the BQ/Cys/ N-GQDs/APTES/FTO electrode was activated for 60 s under a potential of +0.4 V in 0.1 M PBS (pH = 7). Subsequently, the electrode was immersed for 2 h in a 5 mM 3-mercaptopropanoic acid in water. After washing with water, β-Cyclodextrins were finally immobilized by an electropolymerization process (figure S3). The carboxylic terminated electrode was used as a working electrode and immersed in a 5 mM β-Cyclodextrin in 0.1 M PBS (pH = 7). Cyclic voltammetry was performed in the potential range −1.0 V to 1.0 V at 20 mV s^{-1} for 10 consecutive cycles. Finally, the electrode was washed with water and dried under gentle nitrogen flow.

2.3. Measurements by dual-responsive sensor

The proposed sensor was applied to the analysis of both cholesterol and o-toluidine. The host–guest inclusion complexes of β-cyclodextrins with analytes were monitored by electrochemical and fluorescence methods. Thus, voltammetric measurements were conducted in a three-electrode system: the modified FTO electrode was used as the working electrode, while a saturated calomel electrode (SCE) and a Pt wire were used as the reference electrode and the counter electrode, respectively. The potential was swept between −0.4 V to +0.7 V at step of 0.005 V, modulation amplitude of 0.025 V, and a scan rate of 0.01 V s^{-1}.

For fluorescence analysis, fluorescence emission spectra were acquired by exciting the transparent β-CD/COOH/BQ/Cys/N-GQDs/APTES/FTO electrode at a wavelength of 351 nm. Solid fluorescence measurements were performed using a specific approach. Initially, the electrode underwent a pre-incubation step in the presence of the target molecules in solution. Following the pre-incubation, the electrode was carefully extracted from the solution, and subsequent solid fluorescence measurements were conducted.

For cholesterol detection in milk, a saponification step was performed as a pretreatment of milk samples for the extraction of cholesterol according to previous reports [36–39].

3. Results and discussion

3.1. Electrochemical characterization of the assembly process

Cyclic voltammetry and electrochemical impedance spectroscopy measurements were recorded in 0.1 M KCl solution containing 0.5 mM $[Fe(CN)_6]^{3-/4}$.

As shown in Fig. 1A, compared with bare FTO, the current value of APTES/FTO exhibits a significant increase, due to the formation of a positively charged amino terminated layer (NH_3^+) leading to faster electron transfer rate. When the graphene quantum dots were immobilized on the surface of APTES/FTO electrode, the current response noticeably lowers by ≈30%. This is attributed to the negatively charged carboxyl (COO^-) and hydroxyl (OH^-) functional groups present on the surface of N-GQDs which generates the repulsive force to the anionic redox probe. When cysteamine attachment occurs, we can notice an enhancement in the current intensity coupled with the reversibility due

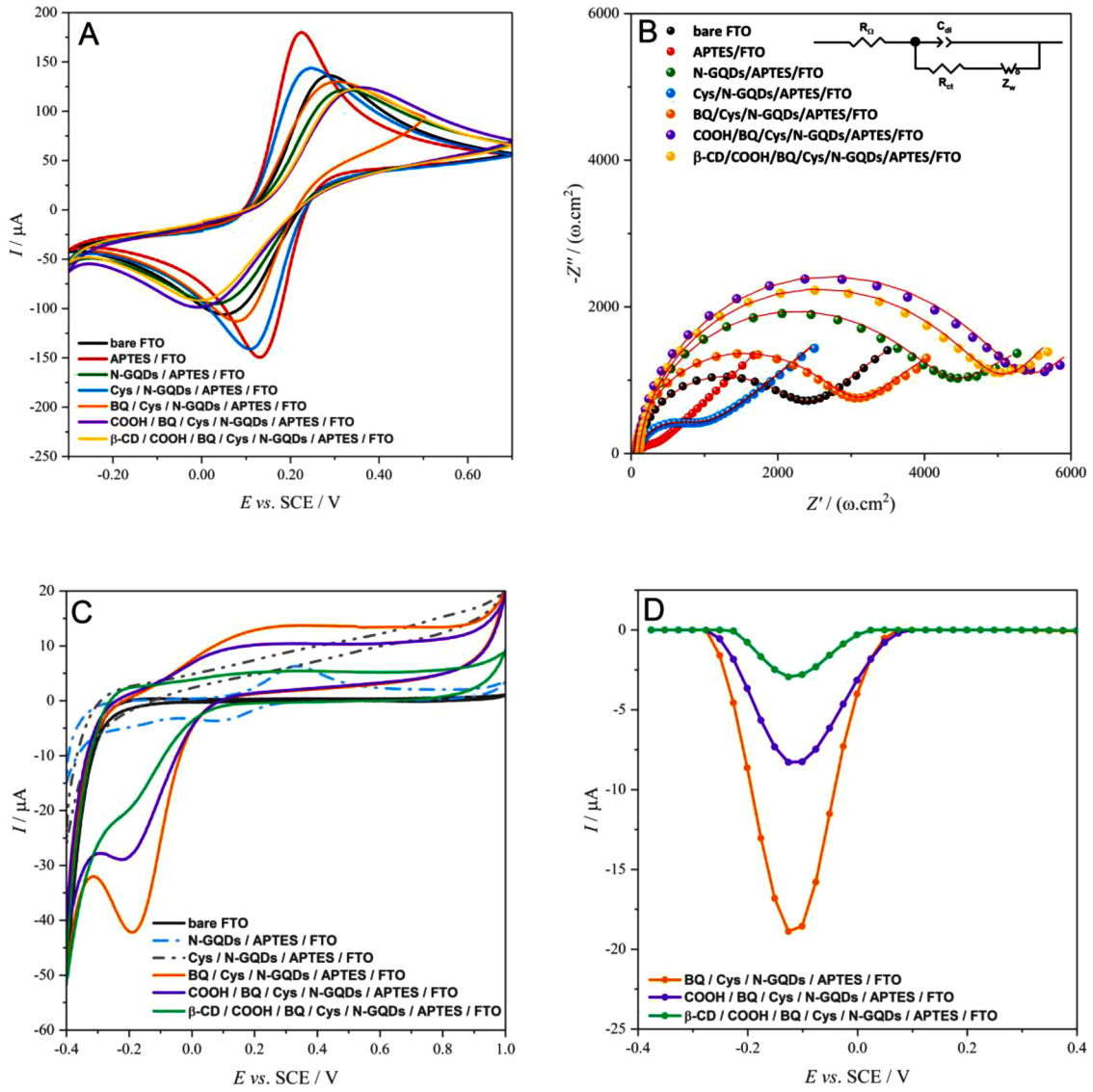

Fig. 1. (A) Cyclic voltammograms of modified electrodes and (B) EIS spectra in a 0.1 M KCl containing 5 mM $[Fe(CN)_6]^{3-/4-}$, (C) cyclic voltammograms and (D) Differential pulse voltammograms of modified electrodes recorded in 0.1 M PBS.

to the thiol terminated assembled layer that ameliorates the electron transport. Incubation in benzoquinone solution leads to an inhibition of the electron transfer between the electrode and the probe. The peak-to-peak separations goes from 140 mV to 220 mV suggesting that BQ moieties are successfully anchored onto the sensing interface. After adding mercaptopropionic acid, the peak current decreased again due to the negatively charged carboxylic acid. Finally, after the immobilization of β-cyclodextrin a slight enhancement in the electron transfer was seen. These results show that β-CD facilitates the access of $[Fe\ (CN)_6]^{3-/4-}$ redox species to the electrode.

EIS measurements were performed and presented in Fig. 1B (Nyquist plots) and Fig. S2 (Bode plots). The impedance values are fitted to standard Randles' equivalent circuit (inset of Fig. 1B) which consist of the Ohmic resistance of the electrochemical cell (R_Ω), surface double-layer capacitance (C_{dl}), charge transfer resistance (R_{ct}), and Warburg impedance (Z_w).

As shown, both R_{ct} and Z_W were in parallel with C_{dl}. This parallel connection caused the semicircle in the Nyquist impedance plot, and the R_{ct} value was directly determined from the diameter of the semicircle. Thus, the variation of R_{ct} value was used as a key parameter for the monitoring of the assembly process (Table S1).

The bare FTO electrode shows a low frequency straight line with a semicircle portion at high frequency region with charge transfer resistance (R_{ct}) of 2.11 KΩ cm^{-2}. The silanization of the FTO surface gives rise to an almost straight line in the impedance plot which is the characteristic of a diffusion-controlled process for the $[Fe\ (CN)_6]^{3-/4-}$ electron transfer reaction. The R_{ct} value drops to 0.21 KΩ cm^{-2}, demonstrating an easy electron transfer to the electrode surface due to the amine terminated generated layer. Yet, the following assembly of N-GQDs obviously enlarge R_{ct} 19 times resulting from the electrostatic repulsion of the $[Fe\ (CN)_6]^{3-/4-}$ probe.

Upon the addition of Cysteamine, the resultant resistance decreases to 0.74 KΩ cm^{-2} with a rise of an almost straight line in the impedance plot which is the characteristic of a diffusion-controlled process for the $[Fe\ (CN)_6]^{3-/4-}$ electron transfer reaction. This result shows not only the successful attachment of cysteamine molecules but highlights the conductivity of the N-GQDs based film. The R_{ct} value increases again at BQ/Cys/N-GQDs/APTES/FTO (2.71 KΩ cm^{-2}) and COOH/BQ/Cys/N-GQDs/APTES/FTO (5.03 KΩ cm^{-2}) due to the strengthened steric hindrance. Finally, the electro-grafting of β-cyclodextrin generates a slight decrease of the resistance (4.72 KΩ cm^{-2}).

Even with the electron transfer through the layers suppressed,

intrinsic electrochemical activity of immobilized BQ can be observed. To investigate the proper electrochemical response of the built system, cyclic voltammograms were recorded in Phosphate buffer solution PBS 0.1 M pH = 7 (Fig. 1C). Upon the Benzoquinone grafting step, CV reveals the presence of an oxidation peak localized at +0.29 V and a reduction peak at −0.19 V relative to the faradic response of benzoquinone. To confirm the immobilization of the probes on the electrode surface, scan rates study was performed (Fig. S4). Therefore, plotting the peaks currents (cathodic and anodic) versus the scan rate shows a linear relationship, suggesting a surface confined electron transfer process. It is worth mentioning that the asymmetric nature of the BQ voltammogram is related to the pH effect on its PCET kinetics. In fact, the asymmetric voltammogram observed was due to the partial protonation of the BQ layer. At pH 7, the benzoquinone layer is expected to be partially deprotonated, but we suggest that some of the quinone groups may still be protonated, leading to an asymmetric voltammogram. The protonated and deprotonated forms of the quinone group have different redox potentials, which can cause the asymmetric voltammogram.

The asymmetry between anodic and cathodic peaks becomes more noticeable as the sweep rate increases. This behavior was found to be in line with previous findings [40].

As expected, the redox signal decreases upon the addition of the different layers; the differential pulse voltammograms (Fig. 1D) are in good agreement with the cyclic voltammograms. The redox signal drops dramatically from −18.9 μA to −2.95 μA proving again the successful anchoring of the β-CDs.

3.2. Optical characterization

N-GQDs exhibit not only excellent electrical conductivity but also enhanced optical properties. A series of experiments were used to investigate the optical properties and surface morphology of N-GQDs in solution (figure S1) and of the FTO substrate.

UV–vis absorption and emission spectra of the as-prepared N-GQDs in water are showed in Fig. 2A. The strong UV–vis absorption peak at 328 nm is assigned to the n–π* transition of C═O and C═N. The absorption band at 219 nm is from the contribution of π–π* transition related to C═C bond. The GQDs solution was light yellow in day light and exhibited strong, bright blue luminescence upon UV irradiation (inset, Fig. 2A). Excitation at 377 nm gives the maximum emission at 410 nm. Once the N-GQDs are immobilized on the electrode surface they maintain their fluorescence at 405 nm (Fig. 2B). Upon the assembly of the system, the fluorescent signal drastically drops although remaining detectable at 401 nm. The final signal was estimated to be sufficient to be used as a fluorescent probe for analytical applications.

3.3. Analytical performances of the sensor

3.3.1. Detection of an electro-active molecule

Ortho-toluidine is adopted for detection of electro-active species. Fig. 3A shows the DPV response of the sensor upon incubation for 5 min in different o-toluidine solutions with concentrations ranging from 1 to 85 μM. As displayed, upon increasing the concentration of o-Toluidine (peak around 0.5 V), a gradual increase of the benzoquinone peak current is observed (peak at 0.047 V). This behavior can be attributed to the gate effect that occurs due to the presence of cyclodextrin that eases the electron transfer between toluidine, benzoquinone, and the electrode. Once the o-toluidine molecules are trapped in the inner cavity of cyclodextrins, an electron transfer occurs from toluidine to benzoquinone causing the re-oxidation of hydroquinone. Thus, the linear concentration-dependent response of benzoquinone was used for the monitoring of o-Toluidine.

As shown in Fig. 3B, two dynamic ranges are revealed with the analytical sensitivity in the low concentration range (1–55 μM) of 0.0966 μA/μM and that in the high concentration range (60–85 μM) of 0.1727 μA/μM.

The detection (LOD) and quantification (LOQ) limits were estimated to be (5.53 ± 0.16) μM ($\sigma/S = 3.29$) and (16.82 ± 0.48) μM ($\sigma/S = 10$), where 'σ ' is the standard deviation of the peak current of the lowest concentration (three runs) and '*S*' is the slope of the calibration graph.

In contrast, increasing the concentration of o-Toluidine was found to engender a uniform decrease in the fluorescence emission intensity of the N-GQDs. Fig. 3C shows the quenching of the N-GQDs fluorescence. A good linear relationship between o-Toluidine concentration and N-GQDs FL response was found (Fig. 3D). Two linear dependances were obtained between 0–60 μM and 60–100 μM with a sensitivity of 432.20 au/μM and 111.87 au/μM, respectively. With the fluorescence method a lower LOD [(5.06 ± 0.15) μM] and LOQ [(15.04 ± 0.45) μM] were reached.

3.3.2. Detection of a non-electroactive molecule

Cholesterol is a non-electroactive molecule with a well-known specific interaction with β-CD [41]. This specific interaction was found to be useful to develop non-enzymatic cholesterol electrochemical sensors as

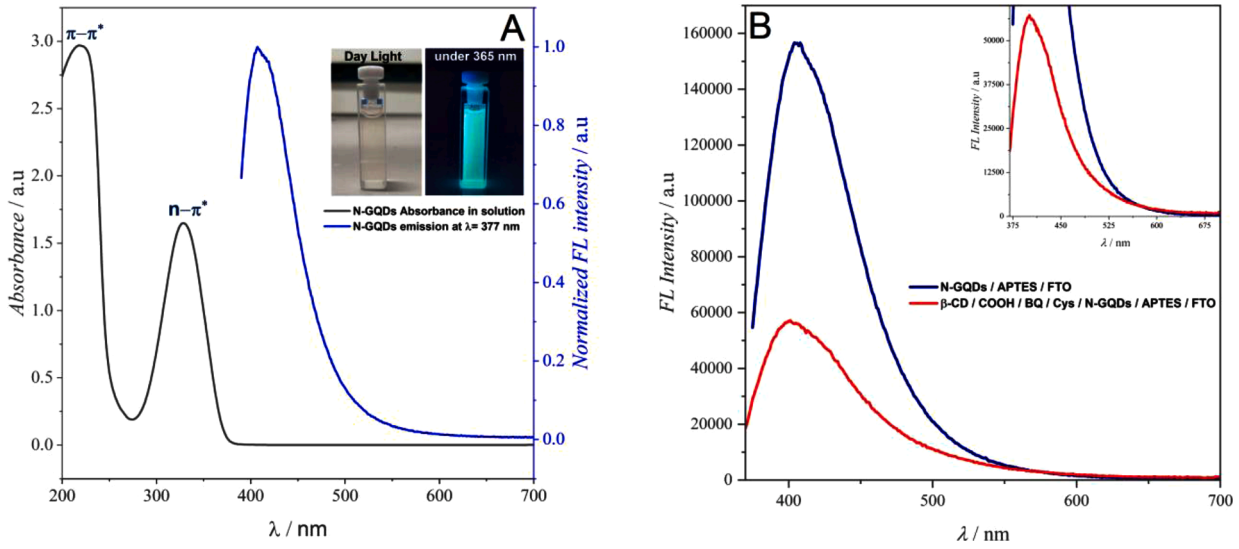

Fig. 2. (A) Fluorescence emission (blue) and UV–vis absorption spectrum (black) of the N-GQDs. The inset shows the photographs of the N-GQDs solution (left) under daylight and 365 nm UV light (right). (B) Fluorescence emission spectra of N-GQDs on FTO substrate.

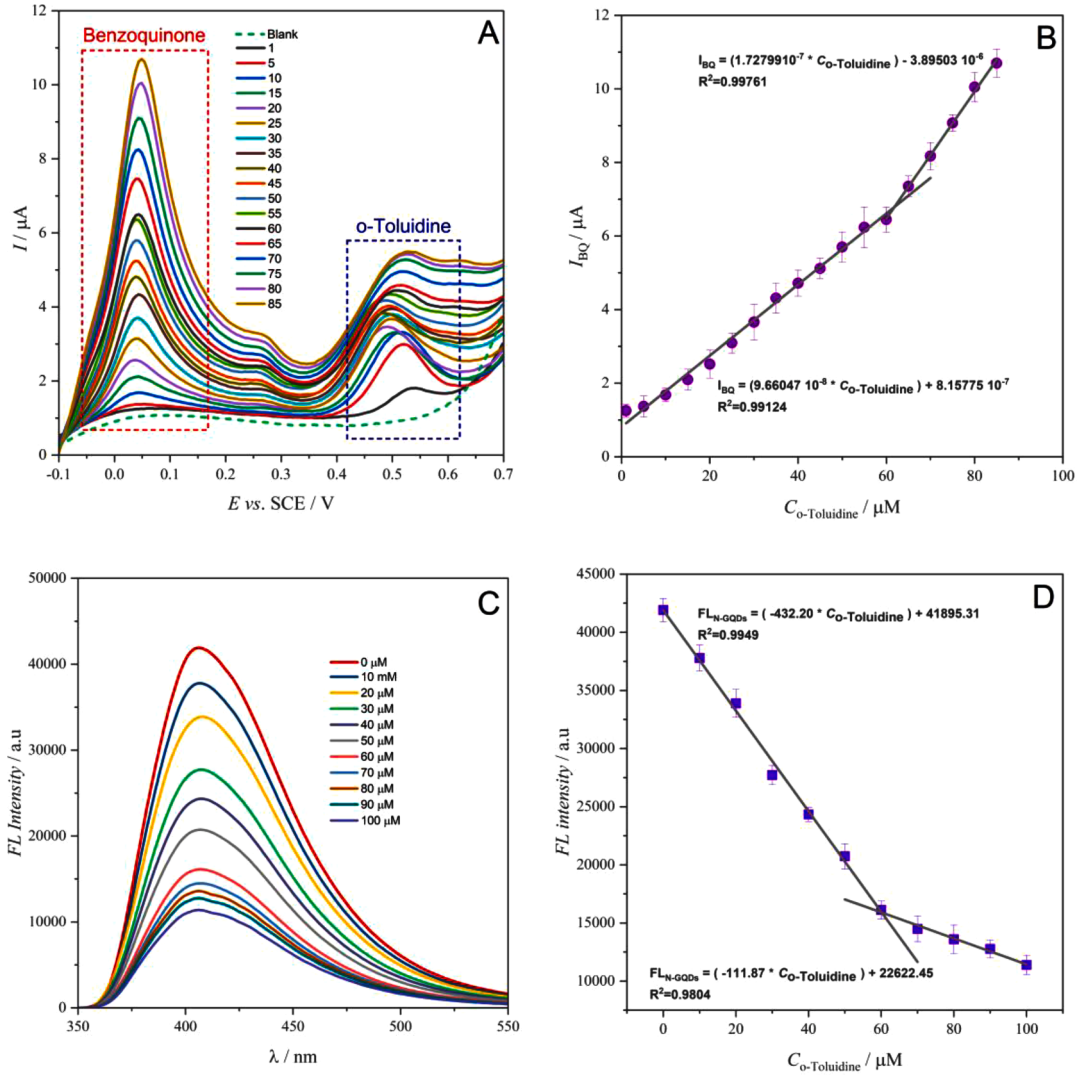

Fig. 3. (A) EC response of the sensor toward different o-Toluidine concentrations and (B) its corresponding correlation plot. (C) FL response of the sensor toward different o-Toluidine concentrations and (D) its corresponding correlation plot.

a replacement of cholesterol oxidase for selective recognition.

Fig. 4A showed the DPV responses at different concentrations. With the addition of Cholesterol, β-CD cavities were blocked gradually to make the reduction peak current of BQ gradually decrease. This phenomenon can be explained by the fact that cholesterol-cyclodextrin complex acts as an inert kinetic barrier for the electron-transfer of the benzoquinone mediator.

A calibration plot was reported in Fig. 4B according to the background subtracted DPVs presented in Fig. 4A inset. A good linear relationship was obtained ranging from 10 to 100 µM. Same as with o-Toluidine, two dynamic ranges are revealed with a sensitivity of 0.07579 µA/µM (10–50 µM) and 0.02007 µA/µM (60–100 µM). Limits of detection and quantification are (2.10 ± 0.042) µM and (6.39 ± 0.13) µM, respectively.

Fluorescence assay showed a similar behavior as in the EC assay. A decrease of the N-GQDs FL response was presented in Fig. 4C. A calibration plot of the fluorescence assay was obtained in the range of 10–100 µM (Fig. 4D), with the limit of detection (LOD) and quantification (LOQ) calculated to be (2.95 ± 0.23) µM and (8.97 ± 0.71) µM, respectively.

Table 1 outlined our approach performances compared to earlier reported chemo/biosensors for cholesterol detection. As can be observed, the merging of the electrochemical and fluorescence transduction modalities did not constrain their analytical performances. The comparison revealed that our bimodal sensor exhibited competitive LODs for cholesterol detection comparable to other cholesterol single-mode sensors and biosensors. More significantly, as compared to earlier dual-mode attempts to detect cholesterol, our sensor has lower detection limits. According to our knowledge, this is the first time an EC/FL approach for cholesterol detection has been proposed.

3.4. Selectivity and stability test

The selectivity ability of the sensor was tested in the presence of common interferences such as ascorbic and uric acid, glucose, NaCl and $CaCl_2$. Histograms of the variation of electrochemical (green) and fluorescence (red) signals are reported in Fig. 5A.

Current (ΔI) and fluorescence (ΔFL) ratios represents the difference in signals between the sensor response in presence of interference toward the initial signal response of the sensor.

A negligible increase in the current and the photo-signal was obtained for glucose, NaCl and $CaCl_2$. In the case of ascorbic and uric acid, a slightly higher increase in the current and photoluminescent response was observed. To verify the stability of the sensor, the electrodes were stored at 4 °C and EC/FL testing was done under optimal condition every 7 days. The results shown in Fig. 5B illustrate that, as the storage time

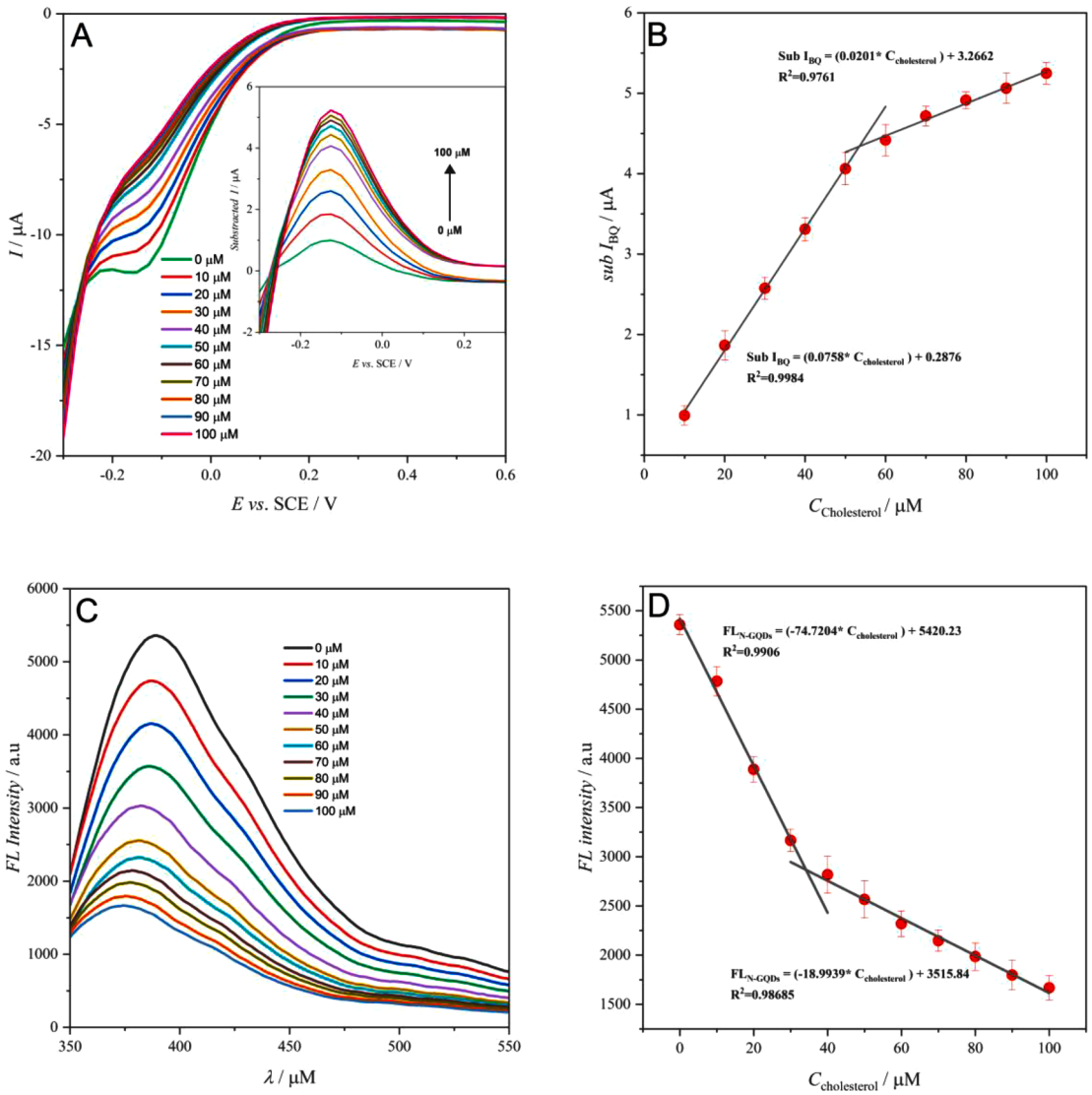

Fig. 4. (A) EC response of the sensor toward different cholesterol concentrations and (B) its corresponding correlation plot. (C) FL response of the sensor toward different cholesterol concentrations and (D) its corresponding correlation plot.

Table 1
Comparison of the analytical performances of the sensor fabricated in this work for cholesterol detection and other cholesterol sensors and biosensors.

Method	Sensing matrix	Linear range (µM)	LOD (µM)	Reference
DPV	Grp-β-CD-MB	1–100	1	[28]
DPV	β-CD/PNAANI/G	1–50	0.5	[42]
Amperometry	MB/β-CD/ Fe3O4/SPCE	0–150	2.88	[38]
Colorimetry	PPy NPs	10–100	3.5	[43]
Fluorometry	Grp/b-CD/ rhodamine 6G	5–30	5	[44]
Fluorometry	β-CD-CQD	0–110	0.7	[45]
Fluorometry	CD-AuNCs	10–100	5.77	[46]
Amperometry	G/Ti(G)-3DNS/	50–8000	6	[47]
PEC	CS/ChOx		10	
Colorimetry	NS-C@PtRu	300–6000	1.4	[48]
Fluorometry		10–2000	129	
photothermal	CS@Pt NS	0–2000	45	[49]
colorimetric			25	
DPV	N-GQDs/BQ/	10–100	2.10	This work
Fluorometry	β-CD		2.95	

became longer, the current value of BQ showed a downward trend. On the other hand, the N-GQDs FL signal showed better stability which was in agreement with previous reports [34]. Although the sensor response slightly decreases, the stability of the constructed sensor remained acceptable over a month.

3.5. Sensor application in real sample

To verify the applicability of the developed sensor in a complex matrix, 2% reduced low fat milk was selected for the detection of cholesterol. The nutritional value of the analyzed milk sample was stated on the back of the packaging. The cholesterol content was stated to be 20 mg per serving (240 cm^3) equivalent to 215.53 µM. The standard addition method was employed to evaluate the apparent recovery of detection. Table 2 shows excellent apparent recovery factors of fluorescence (96.70–101.90%) and electrochemical methods (98.28–102.37%) experimental results with maximum relative error of 2.99%. The recovery values and relative error percentages of the dual-readout sensor are found to be within an acceptable range. This cross-checking reaffirms the reliability of the sensor in accurately detecting the cholesterol concentration in complex matrices such as milk. These results clearly suggest that the proposed sensor device is a promising

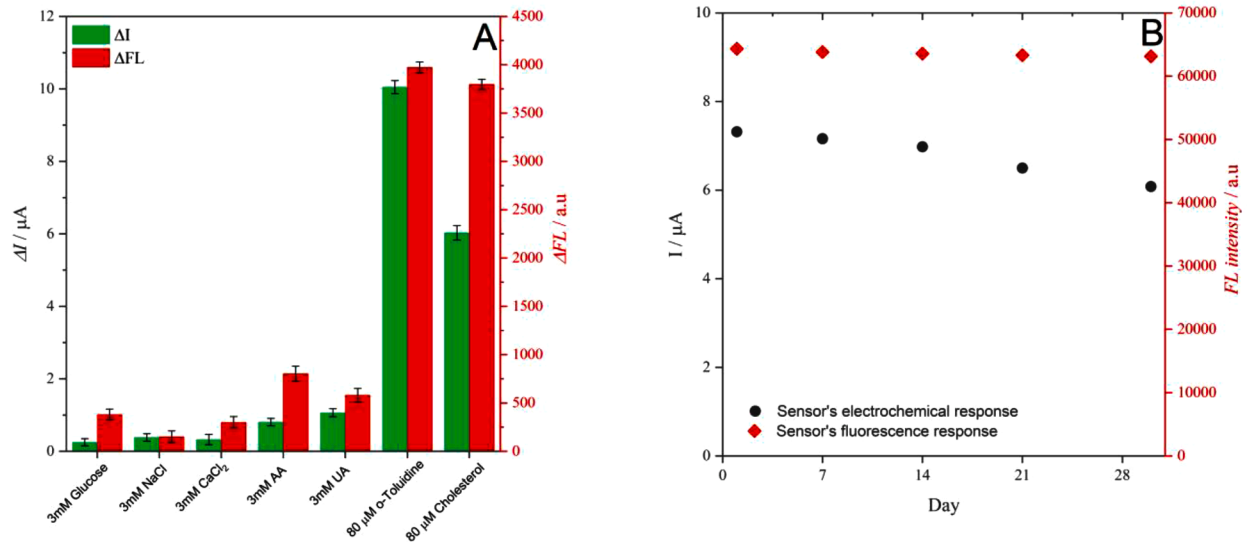

Fig. 5. (A) Selectivity test of the dual-mode electrochemical sensor toward different molecules. (B) Stability test of the EC-FL sensor response.

Table 2
Apparent recovery factors of fluorescence and electrochemical experimental results.

Spiked sample concentration	EC			FL			Expected value
	Found (μM)	Recovery (%)	Relative error%	Found (μM)	Recovery (%)	Relative error%	
0 μM	44,13	102,37	0.83	43,92	101,90	2.93	43 μM
15 μM	57,54	98,68	1.38	57,33	98,20	1.63	
35 μM	77,84	99,38	1.79	77,32	98,18	1.74	
50 μM	92,36	98,28	0.86	91,68	96,70	2.99	

tool for dual mode sensing.

4. Conclusions

In summary, we developed a dual-mode sensor combining electrochemical and fluorescence transduction modes. A hybrid nano-architecture made mainly by N-GQDs, benzoquinone and β-cyclodextrins has been successfully put into use for the detection of both o-toluidine and cholesterol molecules. The unique design of the sensor allowed EC-FL monitoring of the host-guest inclusion complexation between β-CDs and the analytes. The developed sensor demonstrates good performance with excellent sensitivity, good selectivity, and high storage stability. Low LODs were achieved for both o-Toluidine ($LOD_{EC} = 5.53$ μM; $LOD_{FL} = 5.06$ μM) and cholesterol ($LOD_{EC} = 2.10$ μM; $LOD_{FL} = 2.95$ μM). Consequently, the developed bimodal sensor also provides the possibility of accurate determination of cholesterol in milk. Moreover, the reported architecture may become a universal platform for the detection of various molecules which can be recognized by different supramolecules (α- and γ-cyclodextrins, Cucurbiturils, etc.), holding great potential for further applications. Finally, the suggested analytical approach could serve as an inspiration for the creation of more sophisticated dual-readout sensors that would enable more precise and informative assays.

Author Contributions statement

Wafa Aidli: conceptualization and design of the study, acquisition of data, analyses and interpretation of data, drafting of the manuscript.

Abdelmoneim Mars and Ahmed Hichem Hamzaoui: research discussion and revision of the manuscript.

Daniele Marinotto: acquisition, analyses and interpretation of spectroscopic data.

Amedea Manfredi: organic synthesis optimization and discussion of data.

Valentina Pifferi and Luigi Falciola: conceptualization, design and supervision of the study, analysis and interpretation of data, revision of the manuscript, funding raising.

Declaration of Competing Interest

The authors declare the following financial interests/personal relationships which may be considered as potential competing interests:

Wafa Aidli reports financial support was provided by Italian Ministry of Foreign Affairs and International Cooperation (MAECI). Wafa Aidli reports financial support was provided by University of Tunis El Manar.

Acknowledgments

The authors acknowledge the Italian Ministry of Foreign Affairs and International Cooperation (MAECI) for the grant awarded to WA. The authors also acknowledge the University of Tunis El Manar for the mobility grant “Bourse d’Alternance” awarded to WA.

Supplementary materials

Supplementary material associated with this article can be found, in the online version, at doi:10.1016/j.electacta.2023.142936.

References

[1] M.A. Al Mamun, M.R. Yuce, Recent progress in nanomaterial enabled chemical sensors for wearable environmental monitoring applications, Adv. Funct. Mater. 30 (2020), 2005703, https://doi.org/10.1002/adfm.202005703.

[2] S.L. Ullo, G.R. Sinha, Advances in smart environment monitoring systems using iot and sensors, Sensors (Switzerland) 20 (2020) 3113, https://doi.org/10.3390/s20113113.

[3] C. Dincer, R. Bruch, E. Costa-Rama, M.T. Fernández-Abedul, A. Merkoçi, A. Manz, G.A. Urban, F. Güder, Disposable sensors in diagnostics, food, and environmental

monitoring, Adv. Mater. 31 (2019), 1806739, https://doi.org/10.1002/adma.201806739.
[4] H.C. Ates, A. Brunauer, F. von Stetten, G.A. Urban, F. Güder, A. Merkoçi, S.M. Früh, C. Dincer, Integrated devices for non-invasive diagnostics, Adv. Funct. Mater. 31 (2021), 2010388, https://doi.org/10.1002/adfm.202010388.
[5] S.P. Usha, H. Manoharan, R. Deshmukh, R. Álvarez-Diduk, E. Calucho, V.V.R. Sai, A. Merkoçi, Attomolar analyte sensing techniques (AttoSens): a review on a decade of progress on chemical and biosensing nanoplatforms, Chem. Soc. Rev. 50 (2021) 13012–13089, https://doi.org/10.1039/d1cs00137j.
[6] C. Yin, Y. Wang, Q. Zhuang, Dual-ratiometric electrochemical sensor for propyl gallate detection, J. Electroanal. Chem. 880 (2021), https://doi.org/10.1016/j.jelechem.2020.114817.
[7] P. Wu, X. Hou, J.J. Xu, H.Y. Chen, Ratiometric fluorescence, electrochemiluminescence, and photoelectrochemical chemo/biosensing based on semiconductor quantum dots, Nanoscale 8 (2016) 8427–8442, https://doi.org/10.1039/c6nr01912a.
[8] T. Yang, R. Yu, Y. Yan, H. Zeng, S. Luo, N. Liu, A. Morrin, X. Luo, W. Li, A review of ratiometric electrochemical sensors: from design schemes to future prospects, Sens. Actuators, B Chem. 274 (2018) 501–516, https://doi.org/10.1016/j.snb.2018.07.138.
[9] Y. Lu, H. Zhao, G.C. Fan, X. Luo, Coupling photoelectrochemical and electrochemical strategies in one probe electrode: toward sensitive and reliable dual-signal bioassay for uracil-DNA glycosylase activity, Biosens. Bioelectron. 142 (2019), 111569, https://doi.org/10.1016/j.bios.2019.111569.
[10] N. Xia, D. Wu, T. Sun, Y. Wang, X. Ren, F. Zhao, L. Liu, X. Yi, Magnetic bead-based electrochemical and colorimetric methods for the detection of poly(ADP-ribose) polymerase-1 with boronic acid derivatives as the signal probes, Sens. Actuators, B Chem. 327 (2021), 128913, https://doi.org/10.1016/j.snb.2020.128913.
[11] X. Mi, H. Li, R. Tan, Y. Tu, Dual-modular aptasensor for detection of cardiac troponin i based on mesoporous silica films by electrochemiluminescence/electrochemical impedance spectroscopy, Anal. Chem. 92 (2020) 14640–14647, https://doi.org/10.1021/ACS.ANALCHEM.0C03130/ASSET/IMAGES/LARGE/AC0C03130_0006.JPEG.
[12] Q. Han, C. Wang, P. Liu, G. Zhang, L. Song, Y. Fu, Achieving synergistically enhanced dual-mode electrochemiluminescent and electrochemical drug sensors via a multi-effect porphyrin-based metal-organic framework, Sens. Actuators, B Chem. 330 (2021), 129388, https://doi.org/10.1016/j.snb.2020.129388.
[13] D. Liu, S. Meng, X. Shen, Y. Li, X. Yan, T. You, Dual-ratiometric aptasensor for streptomycin detection based on the in-situ coupling of photoelectrochemical and electrochemical assay with a bifunctional probe of methylene blue, Sens. Actuators, B Chem. 332 (2021), 129529, https://doi.org/10.1016/j.snb.2021.129529.
[14] X. Shen, D. Liu, C. Zhu, Y. Li, Y. Liu, T. You, Photoelectrochemical and electrochemical ratiometric aptasensing: a case study of streptomycin, Electrochem. Commun. 110 (2020), 106637, https://doi.org/10.1016/J.ELECOM.2019.106637.
[15] H. Deng, Y. Chai, R. Yuan, Y. Yuan, In situ formation of multifunctional DNA nanospheres for a sensitive and accurate dual-mode biosensor for photoelectrochemical and electrochemical assay, Anal. Chem. 92 (2020) 8370, https://doi.org/10.1021/acs.analchem.0c00918.
[16] F. Nasrin, A.D. Chowdhury, A.B. Ganganboina, O.J. Achadu, F. Hossain, M. Yamazaki, E.Y. Park, Fluorescent and electrochemical dual-mode detection of Chikungunya virus E1 protein using fluorophore-embedded and redox probe-encapsulated liposomes, Microchim. Acta 187 (2020) 1–11, https://doi.org/10.1007/s00604-020-04656-2.
[17] A. Mars, A. Mejri, A.H. Hamzaoui, H. Elfil, Molecularly imprinted curcumin nanoparticles decorated paper for electrochemical and fluorescence dual-mode sensing of bisphenol A, Microchim. Acta 188 (2021), https://doi.org/10.1007/s00604-021-04753-w.
[18] A. Mars, M. Hamami, L. Bechnak, D. Patra, N. Raouafi, Curcumin-graphene quantum dots for dual mode sensing platform: electrochemical and fluorescence detection of APOe4, responsible of Alzheimer's disease, Anal. Chim. Acta 1036 (2018) 141–146, https://doi.org/10.1016/j.aca.2018.06.075.
[19] J. Jia, W. Lu, L. Li, Y. Gao, Y. Jiao, H. Han, C. Dong, S. Shuang, Orange-emitting N-doped carbon dots as fluorescent and colorimetric dual-mode probes for nitrite detection and cellular imaging, J. Mater. Chem. B 8 (2020) 2123–2127, https://doi.org/10.1039/c9tb02934f.
[20] H. Shang, H. Xu, L. Jin, C. Chen, T. Song, C. Wang, Y. Du, Electrochemical-photoelectrochemical dual-mode sensing platform based on advanced Cu9S8/polypyrrole/ZIF-67 heterojunction nanohybrid for the robust and selective detection of hydrogen sulfide, Sens. Actuators, B Chem. 301 (2019), 127060, https://doi.org/10.1016/j.snb.2019.127060.
[21] Y. Ma, A.Y. Chen, X.F. Xie, X.Y. Wang, D. Wang, P. Wang, H.J. Li, J.H. Yang, Y. Li, Doping effect and fluorescence quenching mechanism of N-doped graphene quantum dots in the detection of dopamine, Talanta 196 (2019) 563–571, https://doi.org/10.1016/j.talanta.2019.01.001.
[22] M. Yin, Y. Wan, S. Li, X. Zhao, W. Zhang, Y. Zhang, H. Wang, Carbon nitride-doped melamine-silver adsorbents with peroxidase-like catalysis and visible-light photocatalysis: colorimetric detection and detoxification removal of total mercury, J. Hazard. Mater. 408 (2021), 124978, https://doi.org/10.1016/J.JHAZMAT.2020.124978.
[23] Z. Bagheri, H. Ehtesabi, M. Rahmandoust, M.M. Ahadian, Z. Hallaji, F. Eskandari, E. Jokar, New insight into the concept of carbonization degree in synthesis of carbon dots to achieve facile smartphone based sensing platform, Sci. Rep. 7 (2017) 1–11, https://doi.org/10.1038/s41598-017-11572-8.
[24] J. Shang, Y. Qiao, G. Mao, L. Qian, G. Liu, H. Wang, Bleomycin-Fe(II) agent with potentiality for treating drug-resistant H1N1 influenza virus: a study using electrochemical RNA beacons, Anal. Chim. Acta 1180 (2021), 338862, https://doi.org/10.1016/J.ACA.2021.338862.
[25] Z. Su, H. Xu, X. Xu, Y. Zhang, Y. Ma, C. Li, Q. Xie, Effective covalent immobilization of quinone and aptamer onto a gold electrode via thiol addition for sensitive and selective protein biosensing, Talanta 164 (2017) 244–248, https://doi.org/10.1016/j.talanta.2016.11.049.
[26] W. Yin, A. Grimaud, I. Azcarate, C. Yang, J.M. Tarascon, Electrochemical reduction of CO_2 mediated by quinone derivatives: implication for Li-CO_2 battery, J. Phys. Chem. C 122 (2018) 6546–6554, https://doi.org/10.1021/ACS.JPCC.8B00109/SUPPL_FILE/JP8B00109_SI_001.PDF.
[27] B. Healy, T. Yu, D.C. da Silva Alves, C. Okeke, C.B. Breslin, Cyclodextrins as supramolecular recognition systems: applications in the fabrication of electrochemical sensors, Materials (Basel) 14 (2021) 1668, https://doi.org/10.3390/ma14071668.
[28] N. Agnihotri, A.D. Chowdhury, A. De, Non-enzymatic electrochemical detection of cholesterol using β-cyclodextrin functionalized graphene, Biosens. Bioelectron. 63 (2015) 212–217, https://doi.org/10.1016/j.bios.2014.07.037.
[29] S. Cao, L. Zhang, Y. Chai, R. Yuan, An integrated sensing system for detection of cholesterol based on TiO2–graphene–Pt–Pd hybridnanocomposites, Biosens. Bioelectron. 42 (2013) 532–538, https://doi.org/10.1016/J.BIOS.2012.10.048.
[30] J.C. English, V.S. Bhat, G.L. Ball, C.J. McLellan, Establishing a total allowable concentration of o-toluidine in drinking water incorporating early lifestage exposure and susceptibility, Regul. Toxicol. Pharmacol. 64 (2012) 269–284, https://doi.org/10.1016/j.yrtph.2012.08.011.
[31] G. Cappelletti, V. Pifferi, S. Mostoni, L. Falciola, C. Di Bari, F. Spadavecchia, D. Meroni, E. Davoli, S. Ardizzone, Hazardous o-toluidine mineralization by photocatalytic bismuth doped ZnO slurries, Chem. Commun. 51 (2015) 10459–10462, https://doi.org/10.1039/c5cc02620b.
[32] M.A. Abdel-Rahman, M.F. Shibl, S.H. El-Demerdash, A.M. El-Nahas, First-principle studies on the gas phase OH-initiated oxidation of O-toluidine, Comput. Theor. Chem. 1170 (2019), 112634, https://doi.org/10.1016/j.comptc.2019.112634.
[33] V. Pifferi, G. Cappelletti, C. Di Bari, D. Meroni, F. Spadavecchia, L. Falciola, Multi-walled carbon nanotubes (MWCNTs) modified electrodes: effect of purification and functionalization on the electroanalytical performances, Electrochim. Acta. 146 (2014) 403–410, https://doi.org/10.1016/j.electacta.2014.09.099.
[34] L. Lin, M. Rong, S. Lu, X. Song, Y. Zhong, J. Yan, Y. Wang, X. Chen, A facile synthesis of highly luminescent nitrogen-doped graphene quantum dots for the detection of 2,4,6-trinitrophenol in aqueous solution, Nanoscale 7 (2015) 1872–1878, https://doi.org/10.1039/c4nr06365a.
[35] G. Soliveri, V. Pifferi, R. Annunziata, L. Rimoldi, V. Aina, G. Cerrato, L. Falciola, G. Cappelletti, D. Meroni, Alkylsilane-SiO_2 hybrids. A concerted picture of temperature effects in vapor phase functionalization, J. Phys. Chem. C 119 (2015) 15390–15400, https://doi.org/10.1021/acs.jpcc.5b04048.
[36] V.K. Tandon, H.K. Maurya, On water': unprecedented nucleophilic substitution and addition reactions with 1,4-quinones in aqueous suspension, Tetrahedron Lett. 50 (2009) 5896–5902, https://doi.org/10.1016/j.tetlet.2009.07.149.
[37] A. Hammami, N. Raouafi, V.M. Mirsky, Electrically controlled Michael addition: addressing of covalent immobilization of biological receptors, Biosens. Bioelectron. 121 (2018) 72–79, https://doi.org/10.1016/j.bios.2018.08.044.
[38] S.J. Willyam, E. Saepudin, T.A. Ivandini, β-Cyclodextrin/Fe_3O_4 nanocomposites for an electrochemical non-enzymatic cholesterol sensor, Anal. Methods 12 (2020) 3454–3461, https://doi.org/10.1039/d0ay00933d.
[39] J.H. Ahn, I.S. Jeong, B.M. Kwak, D. Leem, T. Yoon, C. Yoon, J. Jeong, J.M. Park, J. M. Kim, Rapid determination of cholesterol in milk containing emulsified foods, Food Chem. 135 (2012) 2411–2417, https://doi.org/10.1016/J.FOODCHEM.2012.07.060.
[40] W. Zhang, S.M. Rosendahl, I.J. Burgess, Coupled electron/proton transfer studies of benzoquinone-modified monolayers, J. Phys. Chem. C 114 (2010) 2738–2745, https://doi.org/10.1021/jp909540c.
[41] A.B. Ganganboina, R. Doong, Functionalized N-doped graphene quantum dots for electrochemical determination of cholesterol through host-guest inclusion, Microchim. Acta 185 (2018) 526, https://doi.org/10.1007/s00604-018-3063-4.
[42] L. Yang, H. Zhao, S. Fan, G. Zhao, X. Ran, C.-P. Li, Electrochemical detection of cholesterol based on competitive host–guest recognition using a β-cyclodextrin/poly(N-acetylaniline)/graphene-modified electrode, RSC Adv. 5 (2015) 64146–64155, https://doi.org/10.1039/C5RA11420A.
[43] C. Hong, X. Zhang, C. Wu, Q. Chen, H. Yang, D. Yang, Z. Huang, R. Cai, W. Tan, On-site colorimetric detection of cholesterol based on polypyrrole nanoparticles, ACS Appl. Mater. Interfaces 12 (2020) 54426–54432, https://doi.org/10.1021/acsami.0c15900.
[44] A. Mondal, N.R. Jana, Fluorescent detection of cholesterol using β-cyclodextrin functionalized graphene, Chem. Commun. 48 (2012) 7316–7318, https://doi.org/10.1039/C2CC33410K.
[45] Q. Sun, S. Fang, Y. Fang, Z. Qian, H. Feng, Fluorometric detection of cholesterol based on β-cyclodextrin functionalized carbon quantum dots via competitive host-guest recognition, Talanta 167 (2017) 513–519, https://doi.org/10.1016/J.TALANTA.2017.02.060.
[46] W. Xiao, Z. Yang, J. Liu, Z. Chen, H. Li, Sensitive cholesterol determination by β-cyclodextrin recognition based on fluorescence enhancement of gold nanoclusters, Microchem. J. 175 (2022), 107125, https://doi.org/10.1016/j.microc.2021.107125.
[47] S. Komathi, N. Muthuchamy, K.P. Lee, A.I. Gopalan, Fabrication of a novel dual mode cholesterol biosensor using titanium dioxide nanowire bridged 3D graphene

nanostacks, Biosens. Bioelectron. 84 (2016) 64–71, https://doi.org/10.1016/j.bios.2015.11.042.

[48] P.K. Gupta, S.E. Son, G.H. Seong, L-cysteine-meditated self-assembled ptru derived bimetallic metal–carbon hybrid: an excellent peroxidase mimics for colorimetric and fluorometric detection of hydrogen peroxide and cholesterol, Adv. Mater. Interfaces 8 (2021), https://doi.org/10.1002/admi.202101115.

[49] P.K. Gupta, S.E. Son, J. Venkatesan, G.H. Seong, Cauliflower-like platinum nanostructures mediated photothermal and colorimetric dual-readout biosensor for sensitive cholesterol detection, Sens. Actuators B Chem. 386 (2023), 133741, https://doi.org/10.1016/j.snb.2023.133741.